Chemical Synthesis, Structural Modeling, and Biological Activity of the Epidermal Growth Factor-like Domain of Human *Cripto*

Matthias Lohmeyer,[‡] Paul M. Harrison,[§] Subha Kannan,[||] Marta DeSantis,[||] Nicola J. O'Reilly,[⊥] Michael J. E. Sternberg,[§] David S. Salomon,[||] and William J. Gullick*[,‡]

ICRF Molecular Oncology Laboratory, Hammersmith Hospital, Royal Postgraduate Medical School, Du Cane Road, London W12 0NN, U.K., ICRF Biomolecular Modelling Laboratory, 44 Lincoln's Inn Fields, London WC2A 3PX, U.K., Tumor Growth Factor Section, Laboratory of Tumor Immunology and Biology, National Cancer Institute, National Institutes of Health, Bethesda, Maryland 20892, and ICRF Peptide Synthesis, 44 Lincoln's Inn Fields, London WC2A 3PX, U.K.

Received June 25, 1996; Revised Manuscript Received December 19, 1996[⊗]

ABSTRACT: *Cripto*, also known as human teratocarcinoma-derived growth factor 1 (TDGF-1), contains a 40 amino acid region with some similarity to the epidermal growth factor (EGF) domain. However, sequence homology is largely restricted to the classical cysteine/glycine motif with only limited similarities in other regions. Significant differences to human EGF include the absence of all seven residues between the two N-terminal half-cystines and a five-residue shorter loop between the third and fourth half-cystines. We examine the hypothesis that, in spite of these differences, *cripto* can adopt the characteristic EGF-like 1−3, 2−4, 5−6 disulfide bond pattern. A comparative structural model of the growth factor *cripto* was constructed on the basis of its similarity to EGF, transforming growth factor α (TGF-α), and the EGF-like domain of human clotting factor IX. The predicted disulfide bridges and disulfide-bridged loops were analyzed and appear viable in the modeled structure. Moreover, to ascertain the importance of disulfide arrangement for *cripto* bioactivity, two 47-residue peptides were synthesized and then refolded using either a simple oxidative or a controlled sequential refolding protocol. The *cripto* peptides were tested for their ability to stimulate MAP-kinase activity, for inhibition of β-casein induction, and for *Shc* phosphorylation in MDA-MB 453 human mammary carcinoma cells and HC-11 mouse mammary epithelial cells. Data suggest that *cripto* does adopt the 1−3, 2−4, 5−6 disulfide pattern and thus forms the classical EGF-like fold in spite of the significant deletions within the folding domain. The predicted structure of *cripto* shows some of the characteristics of both the ErbB1- and ErbB3/ErbB4-binding growth factors.

Human *cripto* was discovered serendipitously in a cDNA screen for glucose-6-phosphate dehydrogenase which isolated an abnormally long chimeric mRNA (Ciccodicola et al., 1989). The full-length *cripto* mRNA was found to encode a putative 188 amino acid protein. *Cripto* homologues have also been identified in the mouse and in *Xenopus* (Dono et al., 1993; Kinoshita et al., 1995). All *cripto* variants share a 40 amino acid region which has some homology to the EGF-like domain. This characteristic motif is found in the EGF family of growth factors as well as in a diverse variety of other proteins, including blood clotting factors IX, X, and XII, nuclear laminins, *Drosophila melanogaster* Notch protein, human LDL receptor, and the *Caenorhabditis elegans* lin-12 protein, to name only a few.

Subsequent experiments have shown that recombinant full-length *cripto*, as well as a synthetic refolded peptide comprized of the EGF-like domain alone, can act as an autocrine/paracrine factor in a number of different models. *Cripto* stimulated mitogenesis in 184A1N4 human mammary epithelial, SKBR-3 human breast, and the MDA-MB 453 human breast cancer cell lines (Brandt et al., 1994). Other studies have shown that *cripto* expression can transform NOG8 mouse mammary epithelial cells and NIH3T3 cells, which grew in soft agar when transfected with a full-length *cripto* cDNA (Ciardiello et al., 1991; Ciccodicola et al., 1989). Conversely, transfection of *cripto*-expressing GEO and CBS human colon carcinoma cells with antisense *cripto* decreased *cripto* protein levels by 60−70% and depressed growth, soft agar cloning, and tumorigenicity (Ciardiello et al., 1994).

Cripto also appears to be an important tumor marker. When the *cripto* cDNA was discovered, message was only detected in undifferentiated human and mouse teratocarcinoma cells but not in their differentiated counterparts (Ciccodicola et al., 1989). *Cripto* mRNA and protein have subsequently been shown to be present at elevated levels in a large number of human colorectal, gastric, pancreatic, and breast cancers and in premalignant lesions in these tissues (Friess et al., 1994; Gagliardi et al., 1994; Kuniyasu et al., 1994; Panico et al., 1996; Qi et al., 1994). Expression was generally absent or very weak in the surrounding noninvolved tissues (Friess et al., 1994; Gagliardi et al., 1994; Qi et al., 1994). Good correlations with tumor invasiveness have also been reported (Gagliardi et al., 1994), and *cripto* expression was found to be a marker of the metastatic phenotype in ras-transformed rat embryo fibroblasts (Su et al., 1993). Expression of *cripto* in human cell lines appears to be varied (Brandt et al., 1994; Ciccodicola et al., 1989; Kuniyasu et al., 1991; Normanno et al., 1993).

* To whom correspondence should be addressed.
[‡] ICRF Molecular Oncology Laboratory, Hammersmith Hospital, Royal Postgraduate Medical School.
[§] ICRF Biomolecular Modeling Laboratory.
[||] Tumor Growth Factor Section, Laboratory of Tumor Immunology and Biology, NCI, NIH.
[⊥] ICRF Peptide Synthesis.
[⊗] Abstract published in *Advance ACS Abstracts,* March 1, 1997.

S0006-2960(96)01542-5 CCC: $14.00

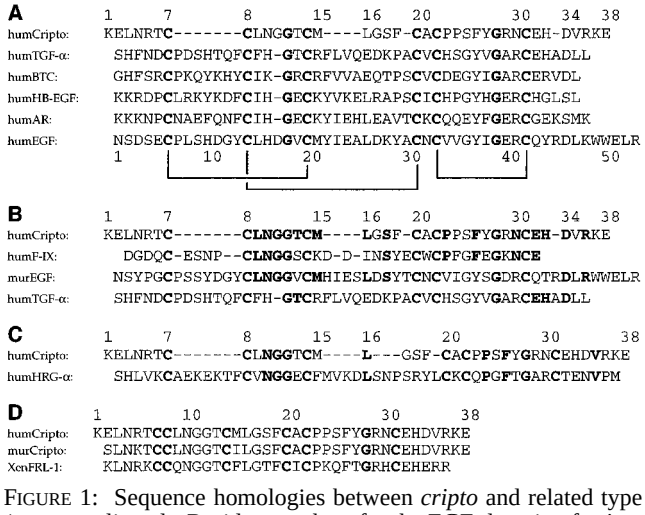

FIGURE 1: Sequence homologies between *cripto* and related type 1 receptor ligands. Residue numbers for the EGF-domain of *cripto* are given above and those for human EGF below their respective sequences. (A) Multiple sequence alignment of human *cripto* with some of the established human ErbB1/EGFR ligands. Residues forming the characteristic cysteine/glycine motif are in bold type. The EGF-like disulfide-bonding pattern is indicated below the alignment. (B) Alignment of the EGF motifs employed for computer homology modeling of *cripto* [EGF domain of human factor IX (humF-IX), murine EGF, and human TGF-α]. Residues conserved with respect to *cripto* are in bold type. (C) *Cripto* and the ErbB4/HER4 ligand heregulin-α. Residues conserved within the two EGF domains are in bold type. (D) Sequences of the other known members of the *cripto* family. The cysteine/glycine motif is shown in bold type.

Thus, although a great deal is known about the expression patterns of *cripto* and some of its biological effects, the cellular target of *cripto* has so far remained elusive. Experiments have shown that *cripto* does not compete with EGF for binding to the EGF receptor (ErbB1, EGFR, HER1; Brandt et al., 1994). Moreover, a number of studies have shown no correlation between ErbB1 status and *cripto* responsiveness or immunohistochemical staining in breast, colon, and gastric carcinoma cells (Brandt et al., 1994; Saeki et al., 1994, 1995). Whether *cripto* interacts with other members of the type 1 growth factor receptor family, such as ErbB2 or the heregulin receptors ErbB3 (HER3) and ErbB4 (HER4), remains to be firmly established.

Clearly, *cripto* shares the EGF-like cysteine/glycine motif found in all type 1 growth factor receptor ligands such as EGF, transforming growth factor α (TGF-α),[1] heparin-binding EGF-like growth factor (HB-EGF), betacellulin (BTC), amphiregulin (AR; Figure 1A), and heregulin-α (HRG-α; Figure 1C). However, in *cripto*, all seven residues between the two N-terminal half-cystines in EGF are absent, and the interval between the third and fourth half-cystines is also five amino acids shorter than in the other growth factors (Figure 1A−C). Moreover, like several isoforms of HRG, the full-length human *cripto* protein does not contain an N-terminal hydrophobic signal sequence or a classical transmembrane domain, whereas these are present in the precursor forms of EGF, TGF-α, AR, HB-EGF, and BTC, as well as in murine *cripto* (Ciccodicola et al., 1989; Dono et al., 1991, 1993). The significance of these differences is not clear.

It is generally assumed that the cysteine motif of *cripto* will fold naturally to the characteristic EGF-like structure (Brandt et al., 1994). In this case, *cripto* might bind to one or more of the type 1 growth factor receptors. However, in many respects, *cripto* appears to be quite different from the established type 1 ligands, and particularly the lack of the first disulfide interval might compromise formation of the characteristic EGF-like disulfide bond fold. Due to the proximity of cysteines 7 and 8 and 20 and 22 in *cripto*, it is not possible to elucidate the disulfide-bonding pattern by conventional techniques involving chemical or enzymatic cleavage and peptide sequencing. Therefore, to characterize the disulfide-bonding pattern in *cripto*, we prepared two samples of the 47 amino acid peptide: one refolded thermodynamically and the other refolded using a staged deprotection and refolding protocol to favor the EGF-like disulfide-bonding pattern. Both of these samples have been compared for potency in *in vitro* cellular assays. To complement these studies, we have investigated the *cripto* structure by computer homology modeling and found that it can assume the predicted 1−3, 2−4, 5−6 disulfide bond pairing of EGF. It is proposed that this configuration represents the biologically active form of *cripto*.

Our examination of the predicted *cripto* structure and evaluation of the extensive previously published site-directed mutagenesis data for ErbB1 ligands suggest that *cripto* shares some of the characteristics of both the ErbB1- and ErbB4-binding growth factors. However, there are also significant differences.

MATERIALS AND METHODS

Peptide Synthesis and Purification. The 47 amino acid peptides were prepared by chemical synthesis using N^{α}-9-fluorenylmethoxylcarbonyl (Fmoc) protected amino acids on an Applied Biosystems 431A peptide synthesizer. The sequence VPPMGIQHSKELNRTCCLNGGTCMLGSFCAC-PPSFYGRNCEHDVRKE corresponds to residues 67−113 of the full-length protein and comprizes the EGF homology domain. For the synthesis of CR47B, all cysteine side chains were triphenylmethyl protected, whereas for CR47C, the second and fourth N-terminal cysteines were protected by acetamidomethyl (ACM) groups. This allowed the selective deprotection and refolding of the 1−3 and 5−6 disulfide bonds before deprotection of the final cysteines and refolding of the peptide to produce the EGF-like 1−3, 2−4, 5−6 configuration (Spetzler et al., 1994). Peptides were purified using a preparative Brownlee C-18 reverse-phase column on a Beckman System Gold high-performance liquid chromatography (HPLC) system. Trifluoroacetic acid (TFA, 0.08%) and a linear gradient of 22.5−34.9% acetonitrile over 50 min at 2 mL/min were used to elute the peptides. Analytical runs were performed on a Brownlee C-18 analytical column using a linear gradient of 22.5−41.4% acetonitrile at 1 mL/min.

Refolding Protocol. Peptide CR47B was refolded using an optimized sulfitolysis/refolding protocol (Spear & Sliwkowski, 1991). The HPLC-purified and lyophilized peptide was dissolved in 6.4 M urea, 0.1 M Na_2SO_3, and 0.02 M

[1] Abbreviations: ACM, acetamidomethyl; AR, amphiregulin; BTC, betacellulin; DIP, dexamethasone, insulin, and prolactin; DMSO, dimethyl sulfoxide; DTT, dithiothreitol; factor IX-EGF, the EGF-like module of human factor IX; FCS, fetal calf serum; HB-EGF, heparin-binding EGF; HPLC, high-performance liquid chromatography; HRG-α, heregulin-α; humEGF, human epidermal growth factor; murEGF, murine epidermal growth factor; RMS, root mean square; SCR, structurally conserved region; TFA, trifluoroacetic acid; TGF-α, transforming growth factor α.

$Na_2S_4O_6$, followed by sequential dialysis in 1 M urea (20 mM Tris, pH 7.1) and 20 mM Tris buffer (pH 7.1). Refolding was performed at room temperature for 16−24 h in the presence of 3 mM cysteine (13.3 mM Tris, 0.03 M sodium borate, 1 mM EDTA, pH 9.0). Refolded peptides were stored at −20 °C. Three batches of CR47B were prepared, and all batches were found to be of comparable quality and bioactivity.

Peptide CR47C was synthesized and refolded essentially as described earlier (Spetzler et al., 1994). The peptide was cleaved from the resin and deprotected with TFA/thioanisole/thiophenol/ethanedithiol/water (82.5:5:5:2.5:5 v/v). This treatment does not remove the ACM-protecting groups from cysteines 2 and 4. The TFA-resin mixture was filtered to remove the resin. Diethyl ether was added to the filtrate to precipitate the peptide which was then filtered on a fine porosity fritted glass funnel. The peptide was subsequently dissolved in 10% formic acid/water and lyophilized. For refolding, the peptide was dissolved in deaerated helium-purged 6 M urea and 0.05 M glycine in 0.1 M Tris buffer, pH 8.5. After sequential dialysis against deaerated 4 and 2 M urea buffers (0.05 M glycine, 0.1 M Tris, pH 8.5), the initial refolding of deprotected cysteines (1, 3, 5, and 6) was initiated by 10-fold dilution of the peptide solution into 20% DMSO, 1 M urea, 0.05 M glycine, and 0.1 M Tris, pH 8.5. The solution was stirred slowly at room temperature for 12 h to allow folding to go to completion. The peptide was then purified by preparative HPLC, as described above, and lyophilized. Removal of the ACM protection groups from cysteines 2 and 4 was performed by dissolving the lyophilized peptide in 10 mL of N_2-purged H_2O/MeOH (6:1, pH 3) and dropwise addition of approximately 5 mL 10 mM I_2 in MeOH. The solution was stirred under nitrogen for 40 min at room temperature. The reaction was quenched by cooling to 0 °C followed by the dropwise addition of 1 M sodium thiosulfate until all remaining color was removed from the solution. Methanol was then removed by rotary evaporation and the peptide purified by semipreparative HPLC, as described above.

Peptide Characterization. The peptides were sequenced using an automated peptide sequencer and analyzed by matrix-assisted laser desorption mass spectrometry. Both CR47B and CR47C possessed identical sequences and were of the correct expected mass of 5181 g/mol. To confirm formation of all three disulfide bonds, refolded peptides were derivatized with 4-vinylpyridine. Free cysteines readily react with 4-vinylpyridine, whereas disulfide-bonded residues do not. The peptides were incubated in a 1% solution of 4-vinylpyridine for 4 h at room temperature and then analyzed by mass spectrometry for derivatized cysteines. Concentrations of the final CR47B and CR47C products were determined by N-terminal sequencing yields.

Cell Culture. MDA-MB 453 human breast carcinoma cells, obtained from the American Type Culture Collection, were cultured routinely in DMEM supplemented with 10% fetal calf serum (FCS). The HC-11 mouse mammary epithelial cell line (a generous gift from Dr. N. E. Hynes, Friedrich Miescher Institute, Basel) was maintained in RPMI-1640 containing 8% heat-inactivated FCS, 5 μg/mL bovine insulin, and 10 ng/mL murine EGF. Cells were free from mycoplasma contamination.

MAP-Kinase Activity. Subconfluent MDA-MB 453 cells, growing in 25 cm^2 flasks, were washed with 0.5% FCS-containing growth medium and grown for a further 24 h before stimulation with *cripto* peptides for 10 min. Following two washes with cold PBS containing 100 μM Na_3VO_4, cells were lysed with 400 μL of lysis buffer (50 μM sodium β-glycerophosphate, 1.5 mM EGTA, 2 mM Na_3VO_4, 1 μM DTT, 2 μg/mL leupeptin, 2 μg/mL aprotinin, 1 μM benzamidine, 1% Nonidet P-40). The lysate was clarified and immunoprecipitated with anti-ERK2 antiserum (serum 122, a generous gift from Prof. Chris Marshall, Chester Beatty Laboratories, London) bound to protein A−Sepharose. The precipitate was washed three times in cold lysis buffer and then suspended in 1 mL of cold kinase buffer (20 mM $MgCl_2$, 2 mM $MnCl_2$, 30 mM Tris-HCl, pH 8.0). The kinase reaction was started by addition of 10 μM ATP, 15 μg of myelin basic protein (MBP, Sigma), and 0.1 μCi of [γ-^{32}P]-ATP (specific activity 2 μCi/μL; Amersham) in 30 μL of kinase buffer. After 30 min at 37 °C, the reaction was terminated by addition of 15 μL of 5× sample buffer containing β-mercaptoethanol and heating at 100 °C for 3−5 min. Samples were analyzed by SDS−PAGE and autoradiography. Band intensities were quantitated by densitometric analysis.

Shc Phosphorylation. HC-11 mouse mammary epithelial cells were maintained as described previously (Hynes et al., 1990). Cells were treated for 5 min with peptide and lysed in 20 mM Tris-HCl (pH 7.5) containing 150 mM NaCl, 1% Nonidet P-40, 5 mM $MgCl_2$, 2 μg/mL aprotinin, 2 μg/mL leupeptin, 1 mM PMSF, 1 mM Na_3VO_4, and 2 mM NaF. The clarified protein lysates were then immunoprecipitated with 2 μg of a rabbit anti-*Shc* antibody (Upstate Biotechnology), separated by SDS−PAGE, and transferred to nitrocellulose. Blots were blocked with 2% dried milk powder in Tris-buffered Tween 20 and probed with a 1:2000 dilution of the anti-phosphotyrosine antibody pY-20 (Transduction Laboratories). The antibody was detected using a 1:5000 dilution of goat anti-mouse IgG conjugated to horseradish peroxidase and visualized by enhanced chemiluminescence (Amersham). Band intensities were quantitated by densitometric analysis.

Induction of β-Casein. To induce β-casein production, HC-11 cells were grown to confluency and then incubated in regular growth medium supplemented with 1 μM dexamethasone, 5 μg/mL bovine insulin, and 5 μg/mL ovine prolactin (DIP induction medium) for 3 days. To test the effects of *cripto* on β-casein induction, EGF was omitted from both the growth and induction media and replaced by different concentrations of CR47B or CR47C. Levels of β-casein were determined by Western blotting, using a 1:5000 dilution of rabbit anti-mouse milk protein antibody (a generous gift from Dr. N. E. Hynes, Friedrich Miescher Institute, Basel). Bound antibody was visualized using a 1:5000 dilution of goat anti-rabbit IgG conjugated to horseradish peroxidase (Amersham). Band intensities were quantitated by densitometric analysis.

Structural Modeling of Cripto. A homology model of *cripto* was constructed on the basis of the known structures of three homologues, using the Biosym modeling package (1992 version) and relevant analysis of disulfides in protein structures (Harrison, 1996). All energy minimizations were performed using the default values for parameters in the consistent valence force field of the Biosym package.

Cripto was modeled as follows: *(i) Identification of Templates.* Coordinates were available in the Brookhaven

Protein Data Bank for three homologues: murine EGF (murEGF; PDB code 1egf; Montelione et al., 1992), human TGF-α (humTGF-α; PDB code 4tgf; Page-Kline et al., 1990), and the EGF-like module of human factor IX (denoted factor IX-EGF; PDB code 1ixa; Baron et al., 1992). Other structures for human EGF (humEGF; Cooke et al., 1987) and heregulin-α (Jacobsen et al., 1996; Nagata et al., 1994) have been solved but were not publicly available at the time of this work. A representative was chosen from the NMR ensemble of murEGF and of humTGF-α, such that no structure in the ensemble was >3.0 Å root mean square deviation (RMS) away from the representative for superimposition over Cα atoms. The Brookhaven coordinates of factor IX-EGF are of a single averaged, energy-minimized structure. Although not a growth factor, factor IX-EGF is the structure with highest sequence identity to *cripto* (54% identity over 28 residues; Figure 1B) and accordingly was used as the template for modeling.

(ii) Identification and Construction of Structurally Conserved Regions. A multiple superimposition of all three known structures was used to identify regions likely to be structurally conserved between the EGF and TGF-α representatives and factor IX-EGF. The RMS values between the three chain traces were 1.5 Å (1egf/1ixa), 1.4 Å (1ixa/4tgf), and 1.8 Å (4tgf/1egf). A structurally conserved region (SCR) was assigned, comprising residues 56−62 and 71−83 in factor IX-EGF. This is equivalent to residues 14−20 and 31−43 in EGF. The part of the factor IX structure that corresponds to this structurally conserved region was used as the template for model construction. The *cripto* sequence was mapped onto the SCR of factor IX-EGF using the Biosym software. The side chains were added for the SCR using rotamers for residues conserved relative to factor IX. Unconserved side chains were given suitable rotamers from the Ponder and Richards rotamer library (Ponder & Richards, 1987). Two deletions relative to factor IX-EGF occur at the β-hairpin residues 14−20 and near the N-terminus residues 7−8 (Figure 1B).

(iii) Construction of the β-Hairpin Deletion (Cripto Residues 14−20). In this region, the *cripto* sequence Met-Leu-Gly-Ser-Phe was modeled as a 3:5 β-hairpin loop (Sibanda et al., 1989; Sibanda & Thornton, 1993), using the Searchloop facility of the Biosym package. The five-residue β-hairpin loop from a bacterial sialidase (1sim, residues 213−217) was chosen. It fitted the site with 0.9 Å RMS for the flanking five residues on the SCRs and accommodated Gly-17 in the L-α conformation. The side chains were given the conformations in the chosen loop. This choice was then melded to the SCRs, and the ω-dihedrals were mended (100 cycles of restrained conjugate gradient minimization, with the charges in the molecule suppressed and keeping all residues fixed, bar residues 13−14 and 20−21 on either side of the loop).

(iv) Construction of the N-Terminal Deletion (Cripto Residues 7−8). In *cripto*, there are no intervening residues between the N-terminal half-cystines of the first two disulfides (Cys-7−Cys-14 and Cys-8−Cys-20), while in factor IX-EGF there are four such residues. To model this region in *cripto*, we used the results of an analysis of sequentially adjacent cystines with a roughly parallel relative orientation in known structures (Harrison, 1996). This suggested that at least one of the cystines in such cystine pairs would be in an α-helical conformation. Accordingly, Cys-7 was constructed with $\phi = -60°$ and $\psi = -40°$. Conjugate gradient minimization was then performed to obtain an allowed cystine rotamer for Cys-7−Cys-14 (200 cycles, with charges suppressed and only the cystine and its flanking residues allowed to move).

(v) The N-Terminus. The six N-terminal residues were left in extended conformation, because of the substantial conformational heterogeneity of the three known structures in that region. Moreover, there is little sequence conservation between *cripto* and any of the three modeling templates at the N-terminus.

(vi) The C-Terminus. The C-terminus, from Glu-32 to Glu-38 was fitted using the appropriate region in TGF-α. Conformations of the *cripto* side chains were assigned with reference to the conserved residues in TGF-α. The structural heterogeneity of the murEGF NMR ensemble for this region precluded its use in modeling *cripto*. The equivalent region from factor IX was also unsuitable, as it comprises only two residues.

(vii) Remaining Side Chains. Remaining side chains in the model were then fitted using the Ponder and Richards side chain rotamer library (Ponder & Richards, 1987). A final energy minimization (100 cycles of conjugate gradients, all explicit charges suppressed) was applied to the whole molecule.

(viii) Structure Verification. The stereochemical quality of the modeled structure and the 1ixa template was evaluated using the program PROCHECK (Laskowski et al., 1993a,b). The *cripto* model has 63% of its (ϕ, ψ) values in the most favored regions of the Ramachandran plot, compared to 53% for the 1ixa structure. Both structures were of comparable stereochemical quality, reflecting the quality expected of structures resolved crystallographically to between 2.5 and 3.0 Å.

RESULTS

Synthesis and Characterization of Cripto Peptides. We have synthesized, purified, and refolded two 47 amino acid peptides comprising the EGF domain of the human *cripto* protein. Adapting a sulfitolysis method, C47B was refolded to its thermodynamically most favorable conformation(s). Refolding of the peptide was accompanied by a mobility shift on the HPLC (Figure 2A), and formation of all three disulfide bonds was further confirmed by mass spectrometry (Figure 2B). Derivatization of the final product with 4-vinylpyridine was unsuccessful, confirming the absence of free cysteine residues (not shown). However, due to the occurrence of two adjacent cysteine residues in the sequence, it was not clear whether the "thermodynamic folding" used to generate CR47B actually produces predominantly the 1−3, 2−4, 5−6 disulfide configuration found in EGF. In theory, 6 cysteines allow for a total of 15 different disulfide isomers, although many will be sterically and thermodynamically unfavorable.

CR47C was synthesized and refolded using a sequential deprotection and refolding strategy designed to direct refolding into the EGF-like configuration. By deprotecting the three cysteine pairs in two stages, the number of theoretically possible isomers was reduced to four (Spetzler et al., 1994). However, these authors have shown that, under such conditions, the 5−6 disulfide is formed very reliably in a number of peptides containing EGF-like motifs and that their refolding protocol, based on knowledge of the EGF refolding

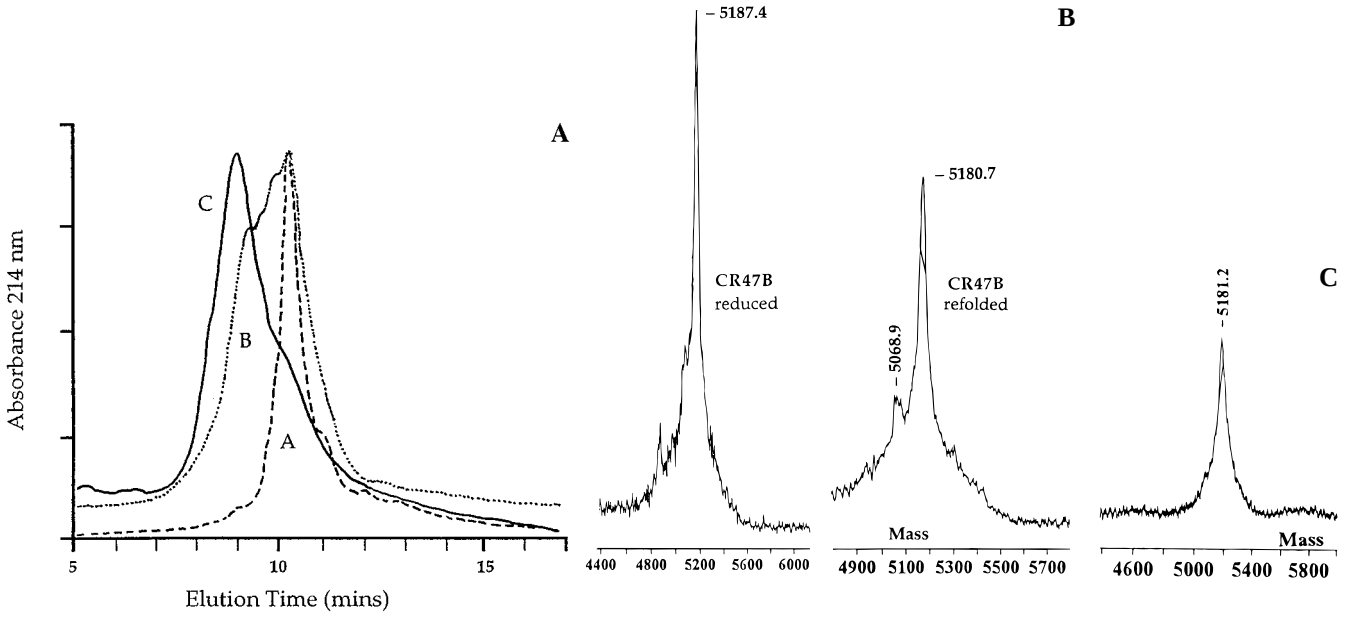

FIGURE 2: (A) HPLC elution profiles for the CR47B peptide before, during, and after the refolding process, showing the fully reduced (A), partially oxidized (B), and fully refolded (C) forms of CR47B, respectively. Refolding and HPLC analysis were performed as detailed in Materials and Methods. Protein folding and disulfide bond formation resulted in a mobility shift from 10.14 to 8.85 min. (B) Laser mass spectrometry of reduced and fully refolded CR47B. The peak masses determined for both species correspond well with the calculated theoretical molecular weights of reduced (5187.64 g/mol) and oxidized (5181.92 g/mol) CR47B, respectively. A minor contaminant with a mass of around 5069 g/mol was identified in the CR47B samples and may represent a peptide lacking a Leu, Ile, Asn, or Asp residue. Treatment of refolded CR47B with 4-vinylpyridine (as detailed in Methods and Materials) did not result in the emergence of higher molecular weight peaks, indicating that all three cystine bonds had been formed. (C) Laser mass spectrometry of refolded CR47C. The peak mass determined corresponds well with the calculated theoretical molecular weight of fully refolded CR47C (5181.92 g/mol). Treatment with 4-vinylpyridine (as detailed in Methods and Materials) failed to derivatize the peptide, indicating the absence of free cysteines.

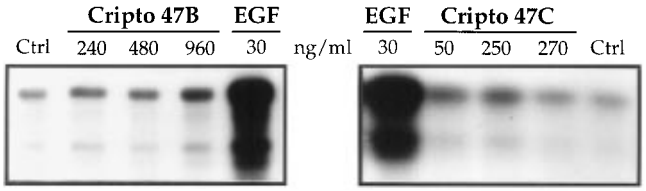

FIGURE 3: Both CR47B and CR47C can activate MAP-kinase. Cells were exposed to different concentrations of the *cripto* peptides, as detailed in Materials and Methods. MAP-kinase-catalyzed phosphorylation of myelin basic protein (upper band) was assessed by autoradiography.

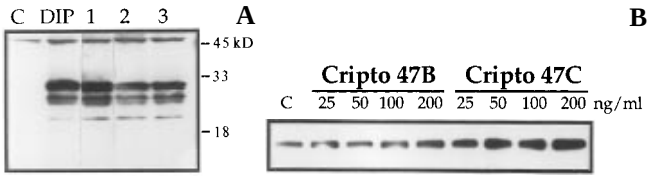

FIGURE 4: (A) CR47C suppresses the induction of β-casein in response to dexamethasone, insulin, and prolactin (DIP). HC-11 cells were grown and induced with DIP as described in Materials and Methods. Cellular proteins were separated by 12% SDS−PAGE and analyzed by immunoblotting with a rabbit serum against mouse milk proteins. The blot shows β-casein (upper doublet ~26 kDa) and the 22 kDa protein X (lower doublet). Lanes: C = uninduced control; DIP = cells induced by treatment with DIP; 1 = cells induced with DIP in the presence of 300 ng/mL CR47B; 2 = cells induced with DIP in the presence of 300 ng/mL CR47C; 3 = cells induced with DIP in the presence of 600 ng/mL CR47C. (B) *Cripto* induces *shc* phosphorylation. HC-11 cells were grown and exposed to *cripto* as described in Materials and Methods. *Shc* phosphorylation was assessed by immunoprecipitation, using an anti-*shc* antibody, and immunoblotting, using the pY-20 anti-phosphotyrosine antibody. Lane C shows basal levels of phosphorylated *shc* in control HC-11 cells.

pathway, allows successful refolding into the 1−3, 2−4, 5−6 configuration with excellent yields (Spetzler et al., 1994). The refolded product was purified by HPLC and checked by mass spectrometry. As with CR47B, derivatization with 4-vinylpyridine was unsuccessful, and the molecular mass of the final product confirmed that all disulfide bonds had been formed (Figure 2C). The correct amino acid sequence of both CR47B and CR47C was confirmed by peptide sequencing (not shown).

MAP-Kinase Activation. The cellular receptor for *cripto* has yet to be identified. Therefore, to assess the effects of *cripto* on cellular signaling systems, CR47B and CR47C were tested for their ability to stimulate phosphorylation of myelin basic protein by MAP-kinase in MDA-MB 453 cell extracts. *Cripto* had previously been shown to stimulate mitogenesis in this cell line (Brandt et al., 1994). Figure 3 illustrates that both CR47B and CR47C are able to stimulate MAP-kinase activity. However, even the maximally achievable response was modest, compared to EGF. The low level of response, together with consistently variable dose−response data, impeded direct potency comparisons between CR47B and CR47C using this assay. This suggests either that MAP-kinase activation is not a major cellular response to *cripto* challenge or that low receptor numbers limit the response amplitude in MDA-MB 453 cells. The full-length *cripto* protein from conditioned medium also activates MAP-kinase in MDA-MB 453 cells (D. Salomon, unpublished experiments).

Inhibition of β-Casein Induction. The two *cripto* peptides were also compared for their ability to inhibit the induction of β-casein and related milk proteins in HC-11 mammary epithelial cells. Figure 4A shows that CR47B at concentrations up to 300 ng/mL did not markedly inhibit the cellular response to DIP induction, whereas CR47C caused a

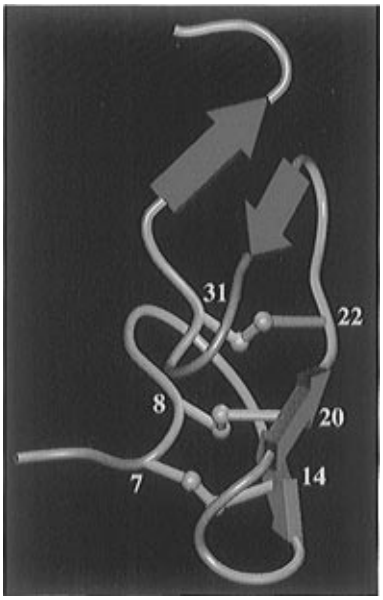

FIGURE 5: View of *cripto* in an orientation that clearly shows the arrangement of disulfide bonds (yellow) relative to the main chain. The six half-cystines are labelled with their respective residue numbers, as defined in Figure 1. The β-hairpins are shown by pairs of red arrows.

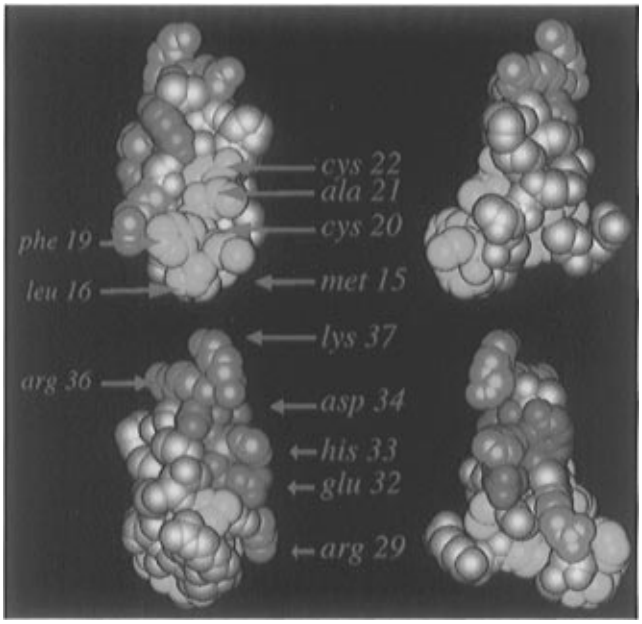

FIGURE 6: A van der Waal's surface representation of the EGF domain of *cripto* (residues 5−38, as numbered in Figure 1A). Positively and negatively charged residues are colored blue and red, respectively. Hydrophobic residues are colored green; the remainder of the molecule is colored gray. Four different views of *cripto* are shown; the image in the top left-hand corner is oriented to present the patch of hydrophobic residues prominently. The other views are clockwise rotations at 90° (top right-hand corner), 180° (bottom left-hand corner), and 270° (bottom right-hand corner). Selected residues comprising the hydrophobic patch and the charged/polar ridge are labeled with their residue type and number. As described in the text, the sizable hydrophobic patch and the charged/polar ridge are centered on opposing sides of the double β-hairpin framework of the EGF-like domain. The importance of individual amino acid side chains for receptor binding is discussed in the text.

pronounced inhibition of β-casein induction. In Figure 4A, for example, densitometric analysis of bands in lanes 2 (300 ng/mL CR47B) and 3 (300 ng/mL CR47C) shows that protein levels were reduced to 77.3% and 43.2% of controls, respectively). However, as with the MAP-kinase assay, quantitative dose−response relationships, required for head-to-head comparisons of the two peptides, proved difficult to establish.

Shc Phosphorylation. *Shc* phosphorylation was found to be a more direct and sensitive indicator of *cripto* activity than MAP-kinase activation or inhibition of β-casein induction. Figure 4B shows the effects of CR47B and CR47C on *Shc* phosphorylation in HC-11 mammary epithelial cells. Maximal stimulation was seen with 200 ng/mL CR47C, increasing band intensity to over 600% of control levels. CR47B at the same concentration increased the intensity of the phosphorylated *shc* band to 234% of control. CR47C achieved a similar level of stimulation (283%) at concentrations of only 25 ng/mL. Clearly, both peptides are active, but CR47C is significantly more potent than the thermodynamically refolded CR47B. This suggests that the active fold for the EGF motif in *cripto* is in the 1−3, 2−4, 5−6 configuration. Thermodynamic refolding of the CR47B peptide may produce a number of species where all three disulfide bonds have been formed but which are less active or inactive compared to *cripto* in the EGF-like configuration.

Molecular Modeling. Overall, the modeled *cripto* structure consists of a closely packed three-disulfide stacked arrangement, with a disulfide β-cross motif (as defined in Harrison & Sternberg, 1996) for the first and second disulfides. Figures 5 and 6 summarize the salient features of the model with respect to main-chain conformation and surface character, respectively. The predicted *cripto* structure contains two β-hairpins of six residues (N-terminal, β13−15, β19−21, and C-terminal, β25−27 and β33−35; Figure 5). The C-terminal *cripto* β-hairpin is equivalent to the single β-bridge found in 1ixa (78−84), but expands to a larger β-hairpin of four to six residues in other, functionally distinct, EGF-like domains [*e.g.*, human e-selectin (1esl; Graves et al., 1994), sheep prostaglandin H2-synthase (1prh; Picot et al., 1994), and human plasminogen activator (1urk; Hansen et al., 1994)]. *Cripto* and humEGF superimpose at 1.25 Å RMS deviation for the main-chain atoms of the structurally conserved region.

Cripto features a hydrophobic surface patch and a ridge of charged residues which are centered on opposing sides of the two β-hairpins (Figure 6). The *cripto* hydrophobic patch is comprized of residues Cys-7, Cys-8, Leu-9, Met-15, Leu-16, Phe-19, Cys-20, Ala-21, and Cys-22 and is reminiscent of the hydrophobic pocket identified in some other receptor ligands, including EGF, TGF-α, and HRG-α (Cooke et al., 1987; Jacobsen et al., 1996; Montelione et al., 1992; Page-Kline et al., 1990). The equivalent residues in human EGF, for example, are Cys-14, Leu-15, Val-19, Cys-20, Met-21, Ile-23, Ala-25, Leu-26, Ala-30, and Cys-31 (Figure 1A,B). The patch includes the conserved methionine and the conserved aromatic at *cripto* positions 15 and 19, respectively. The ridge of mainly charged/polar residues in *cripto* consists of Tyr-27, Arg-29, Glu-32, His-33, Asp-34, Arg-36, Lys-37 and Glu-38. Similar charged "ridges" or "stripes" are found in other EGF-like ligands (Jacobsen et al., 1996).

These general features aside, we have also compared a number of key residues known or suspected to be involved in receptor binding of humEGF, humTGF-α, and heregulin-α with their counterparts in *cripto*. Unfortunately, NMR-

derived structures are inherently imprecise with respect to the side-chain positioning of solvent-exposed residues. Clearly, the same limitation applies to modeled structures derived from NMR structural data. Therefore, discussion of the conformation of exposed side chains important for binding interactions must necessarily be limited to their gross positions. The relative positions of key *cripto* residues in comparison to other type 1 growth factor ligands are shown in Figure 1.

Residues Met-15 and Phe-19 in *cripto* form part of the hydrophobic patch with Phe-19 located adjacent to the ridge of charged/polar residues. Both Met-15 and Phe-19 are conserved or conservatively mutated relative to humEGF (Figure 1A). Mutation of the equivalent residues in human EGF (Met-21 and Tyr-29) reduced binding affinity (Campion et al., 1990; Engler et al., 1987). However, as *cripto* does not appear to bind to ErbB1 receptor homodimers, these conserved residues may be important for general *cripto* ligand structure and/or receptor binding but not for binding specificity.

An aromatic phenylalanine side chain is conserved in *cripto* (Phe-26) and the ErbB4-binding growth factors such as heregulins-α and -*β*. This residue packs on the opposing side to the charged ridge for the C-terminal *β*-hairpin. In the known ErbB1 ligands, the equivalent aromatic residue is a highly conserved tyrosine (Figure 1). However, it is likely that the aromatic residue at this position is important primarily for maintaining structural integrity, as it is the only hydrophobic residue packed on that side of the C-terminal *β*-hairpin.

Arg-41 in human EGF is highly conserved across all of the type 1 growth factor receptor ligands (Figure 1A). Mutagenesis studies have directly implicated this residue in binding interactions and ruled out structural effects by complementary ^{1}H-NMR studies (Hommel et al., 1991). In *cripto*, the equivalent position is occupied by an asparagine residue (Asn-30). However, on examination of the predicted position in the model structure of *cripto*, the neighboring Arg-29 might take on the equivalent role in receptor recognition for *cripto* (Figure 1A).

Another key residue implicated in receptor binding of EGF is Leu-47. Extensive mutagenesis studies with human EGF have shown that replacement of Leu-47 invariably results in significant reductions in receptor binding (Hommel et al., 1991; Matsunami et al., 1991; Ray et al., 1988). In *cripto*, there is a valine at the equivalent position (Val-35), but even this conservative substitution has been shown to decrease receptor binding of EGF significantly (Dudgeon et al., 1990; Ray et al., 1988). Heregulin-α and other ErbB4 binders have a valine which may be considered equivalent to Val-35 in *cripto*.

DISCUSSION

We have synthesized, refolded, and purified two peptides corresponding to the EGF-like domain of *cripto*. CR47B was refolded using a sulfitolysis protocol and has been used previously to study the effects of *cripto* on cellular systems (Brandt et al., 1994). The second peptide, CR47C, was refolded using a sequential deprotection and refolding strategy which greatly favors formation of the EGF-like configuration. Although both CR47B and CR47C activated MAP-kinase, the effect was rather weak, and this suggests that the MAP-kinase pathway may not be central to the activity of the cripto receptor, as demonstrated previously in MDA-MB 453 cells (Brandt et al., 1994) . Alternatively, low receptor numbers may limit the response amplitude of the MAP-kinase assay in MDA-MB 453 cells. Nevertheless, we successfully gauged the relative biological activities of the CR47B and CR47C preparations using the more sensitive *shc* phosphorylation assay. CR47C is about 10 times more potent than CR47B, making CR47C the superior tool for analysis of *cripto*−receptor interactions and downstream signaling. Our results clearly suggest that conventional thermodynamic refolding is suboptimal in the case of the *cripto* EGF domain. More importantly, it strengthens the hypothesis that *cripto* adopts the 1−3, 2−4, 5−6 disulfide pattern and thus forms the classical EGF-like fold.

This finding is supported by our molecular modeling studies, showing that *cripto* can adopt the EGF fold in spite of the two adjacent N-terminal half-cystines and the appreciably shorter loop between the third and fourth cysteines. Moreover, *cripto* displays some notable similarities to the other type 1 growth factor receptor ligands, particularly a large hydrophobic pocket, presumably involved in receptor interactions, and a band of charged residues across the length of the molecule. Both EGF and HRG-α also feature such a ridge of charged residues (Cooke et al., 1987; Jacobsen et al., 1996). However, these charged residues are unlikely to be important for differential binding to the ErbB1 and ErbB4 receptors, as elegant chimeric ligand studies have shown (Barbacci et al., 1995). The hydrophobic domain, however, is likely to play a role in mediating receptor binding. In EGF, mutations in this domain reduce binding affinity without necessarily perturbing the overall ligand structure (Campion et al., 1990, 1993; Koide et al., 1994; Shin et al., 1994; Tadaki & Niyogi, 1993). Moreover, in the only spatially resolved receptor−ligand model, the hydrophobic surfaces of growth hormone have been shown to contribute significantly to binding interactions with the growth hormone−receptor complex (De Vos et al., 1992).

Our model of *cripto* was compared to the known ErbB1 and ErbB4 ligands in the light of established mutagenesis data. The region between half-cystines 8 and 14 in *cripto* is also well conserved in murEGF and HRG-α and thus is unlikely to be important for mediating receptor-specific binding interactions. With respect to potentially important ligand-binding residues in humEGF, such as Met-21, Tyr-29, Tyr-37, Arg-41, Gln-43, Tyr-44, and Leu-47, *cripto* shows less homology to the ErbB1 ligands and appears to be somewhat more related to the ErbB3/ErbB4-binding heregulins (see Figure 1A,C). However, *cripto* lacks the characteristic Ser-His-Leu-Val-Lys N-terminal amino acid sequence important for ErbB4 binding (Barbacci et al., 1995), When transposed to humEGF, this pentapeptide conferred binding specificity to ErbB4 without abrogating ErbB1 binding (Barbacci et al., 1995). Clearly, the absence of a similar sequence in *cripto* suggests that it probably does not bind to ErbB4 homodimers in spite of other apparent similarities.

Another very unusual feature of *cripto* is the absence of the highly conserved arginine immediately prior to the most C-terminal half-cystine of the EGF-like domain. Examination of the predicted structure for *cripto* suggests that Arg-29 may possibly take on an equivalent role in receptor binding for *cripto*.

Overall, *cripto* has some features that are conserved but others that are not conserved relative to ErbB4 and ErbB1 binders. The predicted *cripto* structure is consistent with recent experimental evidence (Brandt et al., 1994) indicating that *cripto* does not act via the ErbB1 receptor pathway. Our studies further suggest that *cripto* is unlikely to interact with receptor *homo*dimers of the other known members of the ErbB family. However, *cripto* may potentially act as an obligate *hetero*dimeric ligand, bridging between two receptors of a heterodimer and interacting with different faces of its surface. Having characterized the refolded ligand in some detail, as presented here, studies are now underway to determine the exact binding specificities of the *cripto* protein.

Alternatively, *cripto* may bind to an as yet undefined member of the type 1 growth factor receptor family. The receptor interface might then be expected to feature some of the characteristics of both the ErbB1 and ErbB4 receptors. However, the discovery of a fifth ErbB receptor is becoming increasingly unlikely, as extensive sequencing efforts have, to date, failed to identify suitable candidates for further members of the ErbB receptor family (Adams et al., 1992, 1993). The hypothesis that *cripto* features an EGF-like fold in order to interact with members of a completely different class of receptors cannot be discounted either at this stage. In fact, Kinoshita et al. recently identified a *cripto* homologue, FRL-1 in *Xenopus laevis*, using a functional screen for tyrosine phosphorylation of the fibroblast growth factor receptor 1 (Figure 1D; Kinoshita et al., 1995). Whether this confirms a direct binding interaction between this receptor and *cripto* remains to be established, as the screen also identified a ribonuclease-related protein, which appears to be an unlikely candidate for an FGF-binding ligand (Kinoshita et al., 1995). As further mouse and human *cripto* analogues are being described, the hunt for the *cripto* receptor continues. Experiments are underway to characterize more clearly whether *cripto* can interact with a novel or previously identified tyrosine kinase receptor.

ACKNOWLEDGMENT

The authors thank Dr. Suhail Islam for his expert assistance with the preparation of Figures 5 and 6.

REFERENCES

Adams, M., Dubnick, M., Kerlavage, A., Moreno, R., Kelley, J., Utterback, T., Nagle, J., Fields, C., & Venter, J. (1992) *Nature 355*, 632−634.

Adams, M., Kerlavage, A., Fields, C., & Venter, J. (1993) *Nat. Genet. 4*, 256−267.

Barbacci, E., Guarino, B., Stroh, J., Singleton, D., Rosnack, K., Moyer, J., & Andrews, G. (1995) *J. Biol. Chem. 270*, 9585−9589.

Baron, M., Norman, D., Harvey, T., Handford, P., Mayhew, M., Tse, A., Brownlee, G., & Campbell, I. (1992) *Protein Sci. 1*, 81−90.

Brandt, R., Normanno, N., Gullick, W. J., Lin, J.-H., Harkins, R., Schneider, D., Jones, B.-W., Ciardiello, F., Persico, M. G., Armenante, F., Kim, N., & Salomon, D. S. (1994) *J. Biol. Chem. 269*, 17320−17328.

Campion, S., Matsunami, R., Engler, D., & Niyogi, S. (1990) *Biochemistry 29*, 9988−9993.

Campion, S., Geck, M., & Niyogi, S. (1993) *J. Biol. Chem. 268*, 1742−1748.

Ciardiello, F., Dono, R., Kim, N., Persico, M. G., & Salomon, D. S. (1991) *Cancer Res. 51*, 1051−1054.

Ciardiello, F., Tortora, G., Bianco, C., M. P., S., Basolo, F., Fontanini, G., Pacifico, F., Normanno, N., Brandt, R., Persico, G. M., Salomon, D. S., & Bianco, A. R. (1994) *Oncogene 9*, 291−298.

Ciccodicola, A., Dono, R., Obici, S., Simeone, A., Zollo, M., & Persico, M. G. (1989) *EMBO J. 8*, 1987−1991.

Cooke, R. M., Wilkinson, A., Baron, M., Pastore, A., Campbell, I., & Sheard, B. (1987) *Nature 327*, 339−341.

De Vos, A., Ultsch, M., & Kossiakoff, A. (1992) *Science 255*, 306−312.

Dono, R., Montuori, N., Rocchi, M., De Ponti-Zilli, L., Ciccodicola, A., & Persico, M. G. (1991) *Am. J. Hum. Genet. 49*, 555−565.

Dono, R., Scalera, L., Pacifico, F., Acampora, D., Persico, M. G., & Simeone, A. (1993) *Development 118*, 1157−1168.

Dudgeon, T., Cooke, R., Baron, M., Campbell, I., Edwards, R., & Fallon, A. (1990) *FEBS Lett. 261*, 392−396.

Engler, D. A., Matsunami, R., Campion, S., & Niyogi, S. (1987) *J. Biol. Chem. 263*, 12384−12390.

Friess, H., Yamanaka, Y., Büchler, M., Kobrin, M. S., Tahara, E., & Korc, M. (1994) *Int. J. Cancer 56*, 668−674.

Gagliardi, G., Talbot, I. C., Northover, J. M. A., Warren, A., Stamp, G. W. H., Lalani, E.-N., Gullick, W. J., & Pignatelli, M. (1994) *Int. J. Oncol. 4*, 865−871.

Graves, B., Crowther, R., Chandran, C., Rumberger, J., Li, S., Huang, K., Presky, D., Familletti, P., Wolitzky, B., & Burns, D. (1994) *Nature 367*, 532−538.

Hansen, A., Petros, A., Meadows, R., Nettesheim, D., Mazar, A., Olejniczak, E., Xu, R., Pederson, T., Henkin, J., & Fesik, S. (1994) *Biochemistry 33*, 4847−4864.

Harrison, P. (1996) Ph.D. Thesis, University College London.

Harrison, P., & Sternberg, M. J. E. (1996) *J. Mol. Biol. 264*, 603−623.

Hommel, U., Dudgeon, T., Fallon, A., Edwards, R., & Campbell, I. (1991) *Biochemistry 30*, 8891−8898.

Hynes, N., Taverna, D., Harwerth, I., Ciardiello, F., Salomon, D. S., Yamamoto, T., & Groner, B. (1990) *Mol. Cell. Biol. 10*, 4027−4034.

Jacobsen, N., Abadi, N., Sliwkowski, M., Reilly, D., Skelton, N., & Fairbrother, W. (1996) *Biochemistry 35*, 3402−3417.

Kinoshita, N., Minshull, J., & Kirschner, M. W. (1995) *Cell 83*, 621−630.

Koide, H., Yokoyama, S., Katayama, Y., Muto, Y., Kigawa, T., Kohno, T., Takusari, H., Oishi, M., Takahashi, S., & Tsukumo, K. (1994) *Biochemistry 33*, 7470−7476.

Kuniyasu, H., Yoshida, K., Yokozaki, H., Yasui, W., Ito, H., Toge, T., Ciardiello, F., Persico, M. G., Saeki, T., Salomon, D. S., & Tahara, E. (1991) *Jpn. J. Cancer Res. 82*, 969−973.

Kuniyasu, H., Yasui, W., Akama, Y., Akagi, M., Tohdo, H., Ji, Z. Q., Kitadai, Y., Yokozaki, H., & Tahara, E. (1994) *J. Exp. Clin. Cancer Res. 13*, 151−157.

Laskowski, R., MacArthur, M., Moss, D., & Thornton, J. (1993a) *J. Appl. Crystallogr. 26*, 283−291.

Laskowski, R., Moss, D., & Thornton, J. (1993b) *J. Mol. Biol. 231*, 1049−1067.

Matsunami, R., Yette, M., Stevens, A., & Niyogi, S. (1991) *J. Cell. Biochem. 46*, 242−249.

Montelione, G. T., Wuthrich, K., Burgess, A., Nice, E., Wagner, G., Gibson, K., & HA, S. (1992) *Biochemistry 31*, 236−249.

Nagata, K., Kohda, D., Hatanaka, H., Ichikawa, S., Matsuda, S., Yamamoto, T., Suzuki, A., & Inagaki, F. (1994) *EMBO J. 13*, 3517−3523.

Normanno, N., Qi, C.-F., Gullick, W. J., Persico, G., Yarden, Y., Wen, D., Plowman, G., Kenney, N., Johnson, G., Kim, N., Brandt, R., Martinez-Lacaci, I., Dickson, R. B., & Salomon, D. S. (1993) *Int. J. Oncol. 2*, 903−911.

Page-Kline, T., Brown, F., Brown, S., Jeffs, P., Kopple, K., & Mueller, L. (1990) *Biochemistry 29*, 7805−7813.

Panico, L., D'Antonio, A., Salvatore, G., Mezza, E., Tortora, G., De Laurentiis, M., De Placido, S., Giordano, T., Merino, M., Salomon, D., Gullick, W., Pettinato, G., Schnitt, S., Bianco, A., & Ciardiello, F. (1996) *Int. J. Cancer 65*, 51−56.

Picot, D., Loll, P., & Garavito, R. (1994) *Nature 367*, 243−249.

Ponder, J. W., & Richards, F. (1987) *J. Mol. Biol. 193*, 775−791.

Qi, C.-F., Liscia, D. S., Normanno, N., Merlo, G., Johnson, G. R., Gullick, W. J., Ciardiello, F., Saeki, T., Brandt, R., Kim, N., Kenney, N., & Salomon, D. S. (1994) *Br. J. Cancer 69*, 903−910.

Ray, P., Moy, F., Montelione, G., Liu, J., Narang, S., Scheraga, H., & Wu, R. (1988) *Biochemistry 27*, 7289−7295.

Saeki, T., Salomon, D., Gullick, W., Mandai, K., Yamagami, K., Moriwaki, S., Takashima, S., Nishikawa, Y., & Tahara, E. (1994) *Int. J. Oncol. 5*, 445−451.

Saeki, T., Salomon, D., Johnson, G., Gullick, W., Mandai, K., Yamagami, K., Moriwaki, S., Tanada, M., Takashima, S., & Tahara, E. (1995) *Jpn. J. Clin. Oncol. 25*, 240−249.

Shin, S., Watanabe, M., Kako, K., Ohtaki, T., & Munekata, E. (1994) *Life Sci. 55*, 131−139.

Sibanda, B. L., & Thornton, J. (1993) *J. Mol. Biol. 229*, 428−447.

Sibanda, B. L., Blundell, T., & Thornton, J. (1989) *J. Mol. Biol. 206*, 759−777.

Spear, K. L., & Sliwkowski, M. X. (1991) in *Techniques in Protein Chemistry* (Villafranca, J. J., Ed.) Academic Press, New York.

Spetzler, J. C., Rao, C., & Tam, J. P. (1994) *Int. J. Pept. Protein Res. 43*, 351−358.

Su, Z. Z., Austin, V. N., Zimmer, S. G., & Fisher, P. B. (1993) *Oncogene 8*, 1211−1219.

Tadaki, D., & Niyogi, S. (1993) *J. Biol. Chem. 268*, 10114−10119.

BI961542P